

UNCLASSIFIED

AD **4 3 7 8 6 4**

---

DEFENSE DOCUMENTATION CENTER

FOR

SCIENTIFIC AND TECHNICAL INFORMATION

CAMERON STATION, ALEXANDRIA, VIRGINIA



UNCLASSIFIED

NOTICE: When government or other drawings, specifications or other data are used for any purpose other than in connection with a definitely related government procurement operation, the U. S. Government thereby incurs no responsibility, nor any obligation whatsoever; and the fact that the Government may have formulated, furnished, or in any way supplied the said drawings, specifications, or other data is not to be regarded by implication or otherwise as in any manner licensing the holder or any other person or corporation, or conveying any rights or permission to manufacture, use or sell any patented invention that may in any way be related thereto.

File Copy #1  
Do Not Remove  
code 3

1

437864

EXPERIMENTAL VERIFICATION  
OF  
SUN POWERED LASER TRANSMITTER

Interim Engineering Report #2  
Project Director E. O. Dixon

Contract Nr. AF33(657)-8619  
Project Nr. 4335; Task Nr. 433513

RESEARCH CENTER

American  Optical  
COMPANY

Southbridge, Massachusetts

1958

The applied research reported in this document has been made possible through support and sponsorship extended by the Electromagnetic Warfare and Communications Laboratory of the Aeronautical Systems Division under Contract Nr. 33(657)-8619. It is published for technical information only, and does not necessarily represent recommendations or conclusions of the sponsoring agency.

5. *Experimental Verification*  
*of*  
*Sun Powered Laser Transmitter*

(6) EXPERIMENTAL VERIFICATION  
of  
SUN POWERED LASER TRANSMITTER •

(9) Interim Engineering Report <sup>No.</sup> 2, Aug - Nov 62,  
Project Director E. O. Dixon

(10) by J. A. [illegible], G. R. [illegible] and M. R. [illegible]

(15) Contract ~~Nr~~ AF33(657)-8619  
(16) Project ~~Nr~~ 43358 Task ~~Nr~~ 433513  
(17) \_\_\_\_\_

1958

*CP*


The applied research reported in this document has been made possible through support and sponsorship extended by the Electromagnetic Warfare and Communications Laboratory of the Aeronautical Systems Division, under Contract Nr 33(657)-8619. It is published for technical information only, and does not necessarily represent recommendations or conclusions of the sponsoring agency.

## ABSTRACT

✓ This second Interim Engineering Report published under Contract Nr. AF33(657)-8619 describes the continuing effort of experimentation and design leading to the delivery of an experimental model of a sun-powered laser transmitter.

The design and fabrication of the transmitter is discussed with respect to the optical system and mount.

An experimental Nd-doped  $\text{CaWO}_4$  Laser is described. Related to this description are integral pump optics requirements, fabrication problems and thermal considerations of the unit. ~~Evaluation of commercial Nd-doped  $\text{CaWO}_4$  crystals was begun.~~

Finally, ✓ experimental Nd-doped glass lasers are discussed in both the short- and long-fiber configurations. 

## TABLE OF CONTENTS

### PAGE

Abstract	ii
Table of Contents	iii
List of Illustrations	iv
Forward	v

1	<u>INTRODUCTION</u>	1
2	<u>WORK ACCOMPLISHED</u>	3
2.1	DESIGN AND FABRICATION OF SUN-POWERED LASER TRANSMITTER	3*
2.1.1	<u>Optics</u>	3
2.1.1	<u>Mount</u>	4
2.2	EXPERIMENTAL Nd-DOPED $\text{CaWO}_4$ LASER	7
2.2.1	<u>Pump Optics</u>	7
2.2.2	<u>Laser Cavity</u>	11
2.2.3	<u>Heat Sink and Cooling System</u>	13
2.2.4	<u>Evaluation of Laser Materials</u>	17
2.2.5	<u>Thermal Conductivity Measurements</u>	18
2.2.6	<u>Calculation of Temperature Gradients</u>	22
3	<u>EXPERIMENTAL Nd-DOPED GLASS LASER</u>	30
3.1	SHORT FIBER LASER	31
3.2	LONG FIBER CONFIGURATION	32

## LIST OF ILLUSTRATIONS

<u>FIGURE</u>		<u>PAGE</u>
1.	Folded Mirror System	5
2.	Mirror Mount and Center Section Modification	6
3.	Redesigned Pump Optics for Calcium Tungstate	8
4.	Sketch Showing Retroreflection of Incident Pump Light	9
5.	Pump Optics Using Cone Condensor in Place of Hyperhemispherical Aplanat	10
6.	Hollow Milling Tool	12
7.	Polishing Lap	14
8.	Heat Sink and Heat Exchanger System	15
9.	Die Cavity for Forming Sintered Silver Indium Heat Sink	16
10.	Active Measurement Technique for Determining Internal Loss Coefficients of $\text{CaWO}_4$ Crystals	18
11.	Thermal Conductivity Measurement Apparatus	20
12.	Thermal Conductivity Depression from Pure Cast Silver	23
13.	Radial Temperature Distribution	27
14.	Immersion Optics and End Pumping Scheme Modified for Nd-doped Fiber Laser	32
15.	Pump Optics for Long Fiber	34

# FORWARD

The following senior people in the Research Center of the American Optical Company have contributed in a major way to the work effort under Contract AF 33(657)-8619.

D. A. LaMarre

G. R. Simpson

M. R. Thorburn



## 1 INTRODUCTION

Interim Engineering Report #2 describes the work accomplished at the American Optical Company in the period from August through November, 1962, under Contract AF33(657)8619. This contract, monitored by Mr. D. Matulka, AFSC, Aeronautical Systems Division, Wright-Patterson Air Force Base, Ohio, calls for a one-year program of experimentation and design, leading to the delivery of an experimental model of a sun-powered laser transmitter. The initial contract effort performed in the period April to August, 1962, has been reported in Interim Engineering Report #1.

The program which is underway, and which will be carried out insofar as possible under the referenced contract may be divided in the following way:

- 1) analytical work leading to the selection of the best laser materials now available for the sun-powered application
- 2) the development of necessary fabrication techniques, and the design and fabrication of laser cavities and integral pump optics from the chosen materials
- 3) experimental evaluation of the laser material, including operation from a sun-simulating pump source
- 4) the design and construction of a sun-tracking laser transmitter which will supply pump power and cooling for the experimental laser cavities
- 5) experimental evaluation of the sun-powered laser transmitter.

The major portion of the initial program effort reported in Interim Engineering Report #1 fell into categories 1) and 4), above. As a result of this analytical effort, and previous work performed under Contract AF33(616)-8025, the neodymium-doped laser materials (particularly calcium tungstate, and secondly, glass) were selected as the best candidates for sun-powered laser operation. An important consideration here was the need for operation at relatively high temperatures (approaching room temperature) in any outer space applications, in order that heat by-products could be rejected into outer space with practical radiator designs.

The mid-program effort which is described in the following pages falls into the first four categories listed, with the important emphasis on the experimental evaluation of laser materials, the development of necessary fabrication techniques, and the construction of the transmitter mount.

## 2 WORK ACCOMPLISHED

### 2.1 DESIGN AND FABRICATION OF SUN-POWERED LASER TRANSMITTER

#### 2.1.1 Optics

The design of the sun-powered laser transmitter was begun early in the contract period, and the major aspects of that design have been discussed in Interim Engineering Report #1. The optics design, as described there, consists of a primary collector, a 24 inch diameter F/1.5 ( $NA = 0.33$ ) paraboloid, and one or more aplanatic refracting elements whose design is determined by the particular laser material in use. The refractors, of course, operate to increase the system numerical aperture to a number approximately equal to the refractive index of the laser material.

Tinsley Laboratories, Berkeley, California were selected as suppliers of the primary mirror, based on price and delivery quotations. In this report period, the mirror has been figured, aluminized, and SiO overcoated at Tinsley, and received at the American Optical Company.

One major change has been made in the original design of the optical system, as a result of a study of the spectral filtering problem. Spectral filtering of the collected sun's energy so that only useful pump energy reaches the laser material will greatly ease the laser cooling problem. For the neodymium-doped laser materials, the bulk of the useful pump energy lies in the spectral region between 500 and 900 m $\mu$ . Absorption filters exist which have sharp rises in transmission in the 500 m $\mu$  region, but none are known which have sharp decreases in transmission in the 900 m $\mu$  region. Iron-doped glasses perhaps are the nearest approximation to the long wavelength absorption filter desired, but they do exhibit a substantial amount of absorption in the 700 to 900 m $\mu$  region where a considerable fraction of the useful pump energy lies. The use of absorption filters, then, would reduce the overall system performance appreciably, in addition to introducing the not negligible problem of cooling the filters themselves, because of the significant amount of sun's energy to be absorbed.

Another, more attractive, approach to spectral filtering is the employment of multi-layer interference filter of the dichroic type. "Cold-mirror" band-pass designs exist which are highly reflecting over a wide region of the spectrum and highly transmitting in the remaining region, with negligible absorption except perhaps in the UV region. By utilizing a large number of interfering layers, and by careful design, it is possible to get very sharp cut-on and cut-off characteristics.

A quotation of \$2500.00 was obtained from Optical Coating Laboratories, Incorporated, Santa Rosa, California, for the deposition of a cold mirror interference filter on the 24" primary mirror, which would reflect 95% of the collected energy between 500 and 900 mμ, and transmit 90% of the energy at shorter and longer wavelengths. Since this cost was approximately equal to that of the mirror itself, and since it would be necessary to strip and recoat the primary mirror to match the pumping region of any new choices in laser material, it was decided that this approach was prohibitively expensive.

It is obvious, of course, that an elaboration of the optical system would permit greater freedom in the placement of a spectral filter. For this reason, therefore, it was decided to fold the system using a plano secondary mirror. The primary would then be aluminized, and the smaller, less expensive, and more accessible secondary would carry the interference filter. Such a system was designed and is illustrated in Figure 1. The secondary is placed as far from the primary as possible for minimum vignetting of the sun's energy (8%, calculated). The secondary plano has been completed, coated, and delivered to American Optical Company. Cost of coating the smaller secondary was about 15% of the estimated cost of coating the primary mirror.

### 2.1.2 Mount

In this report period, the design of the transmitter mount, as described in Interim Engineering Report #1, has been completed. Fabrication and assembly of the mount is complete except for painting, balancing, and optical alignment.

The mirror mount and center section (Figure 2) have been modified to accept the folded version of the optical system described in the previous section. A webbed member with adjustments for optical alignment has been mounted on the center section to support the dichroic-coated optical flat. The laser unit tube is supported at one end on the mirror cell, with

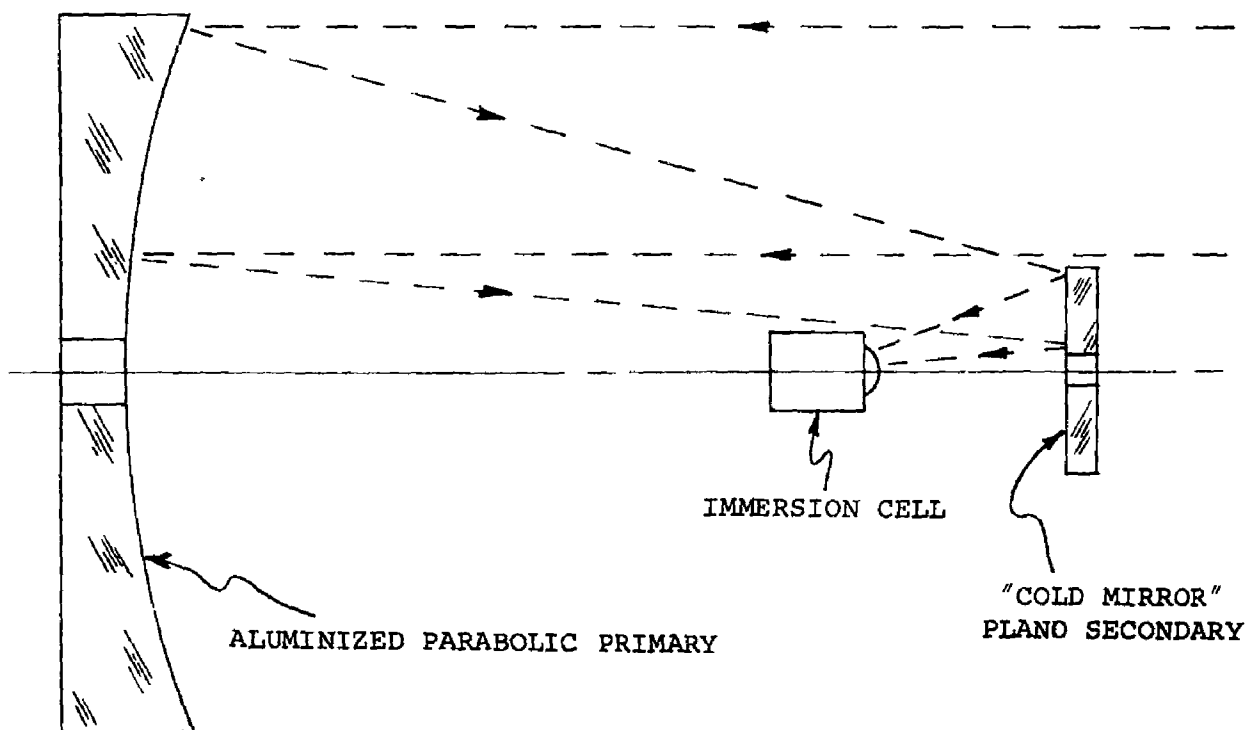


Figure 1. Folded Mirror System

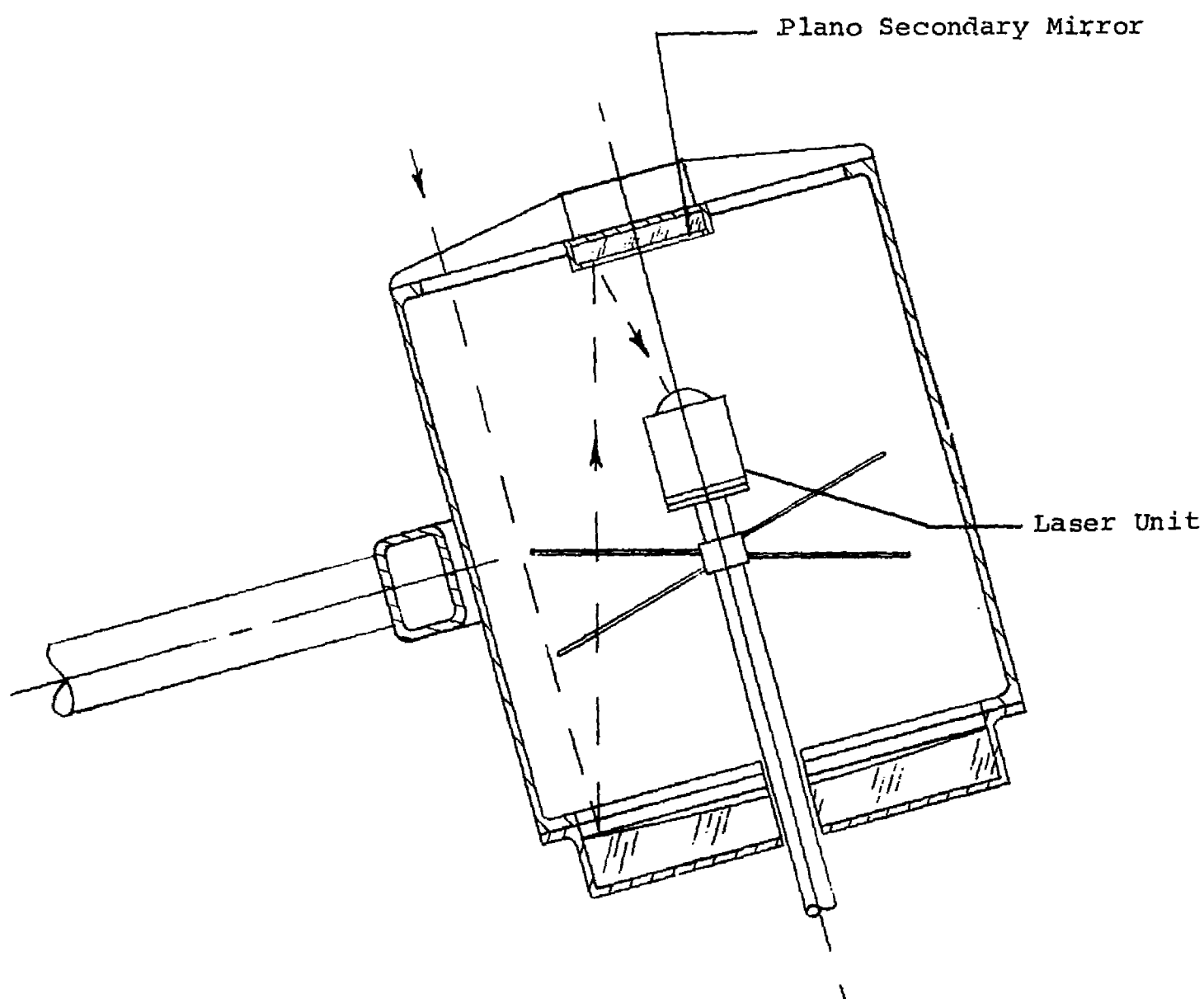


Figure 2. Mirror Mount and Center Section Modification

lateral stability maintained by tie rods at the flanged end. This design permits lateral and axial adjustment and a relatively easy method of changing the laser unit. The tubular support also contains the double-walled flexible tubing through which coolant is circulated to the laser cavity heat sink and heat exchanger described in a following section.

## 2.2 EXPERIMENTAL Nd-DOPED $\text{CaWO}_4$ LASER

### 2.2.1 Pump Optics

The optics of the end pumped configuration which was developed for ruby laser material under the previous contract has been redesigned to take advantage of the high refractive index of calcium tungstate. Figure 3 illustrates the newer design, scaled for the system based on a 24" diameter collector. The refractors have been designed in a higher index flint glass, and the nominal NA of the system is now 1.9. The diameter of the immersion hemisphere has been reduced as much as possible in the  $\text{CaWO}_4$  in order that the entire tungstate piece including hemisphere can be of doped material. This is an alternate design approach which avoids the uncertainties of obtaining a clear-doped integral piece in high quality. Design optimization considered the increased aberration losses of a smaller hemisphere, and the greater fraction of pump light absorbed (and therefore wasted), in a larger hemisphere.

Although the design just discussed is efficient optically, a serious mechanical fabrication difficulty is intrinsic with this design. To efficiently trap the pump energy at the intersection area to a sharp  $90^\circ$  angle. Any fillet residual at this intersection results in a retroreflection of the incident pump light as illustrated in the sketch below. (Figure 4). Because of the fragility of  $\text{CaWO}_4$ , this lapping operation is extremely difficult to accomplish.

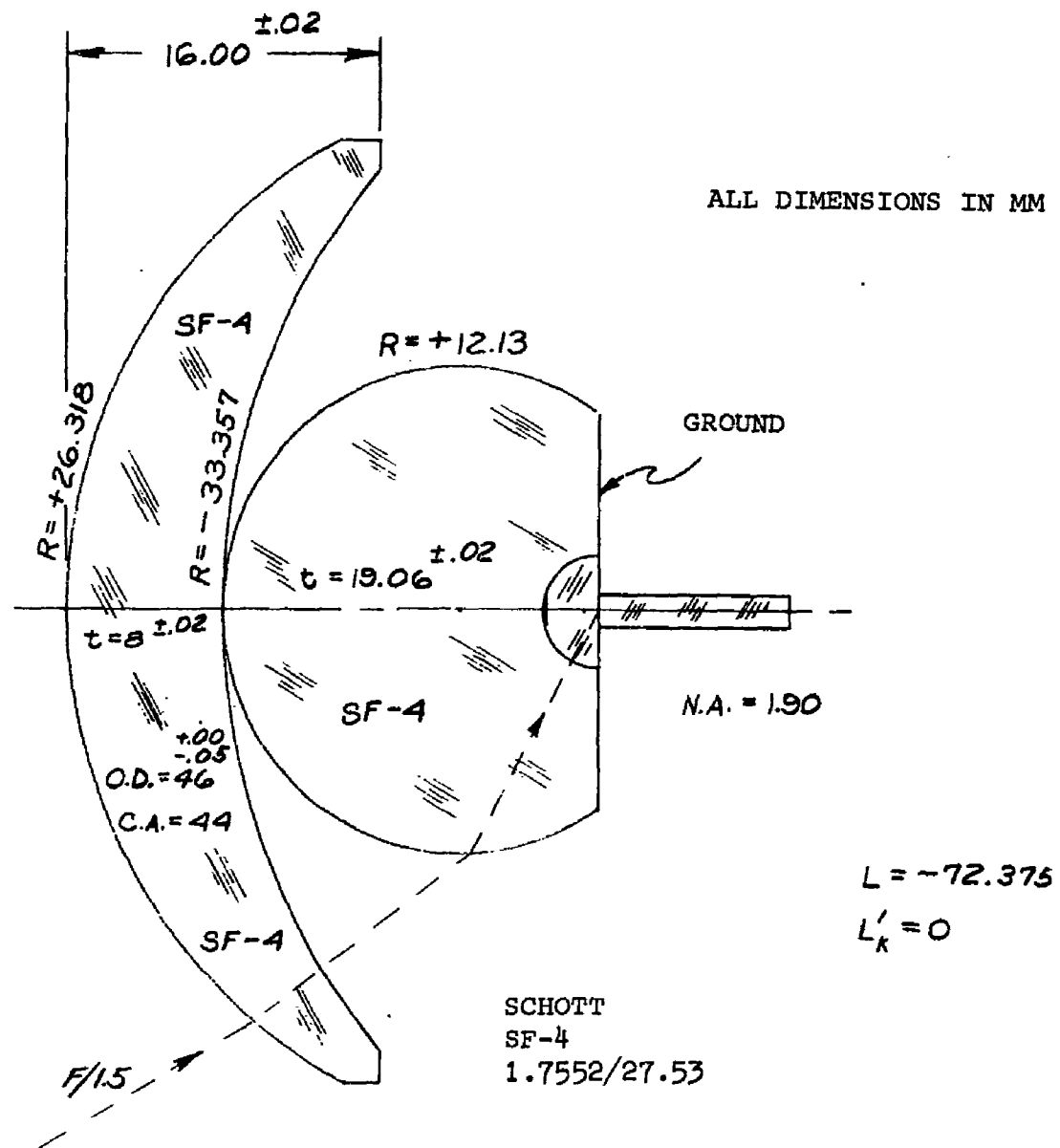


Figure 3. Redesigned Pump Optics for Calcium Tungstate



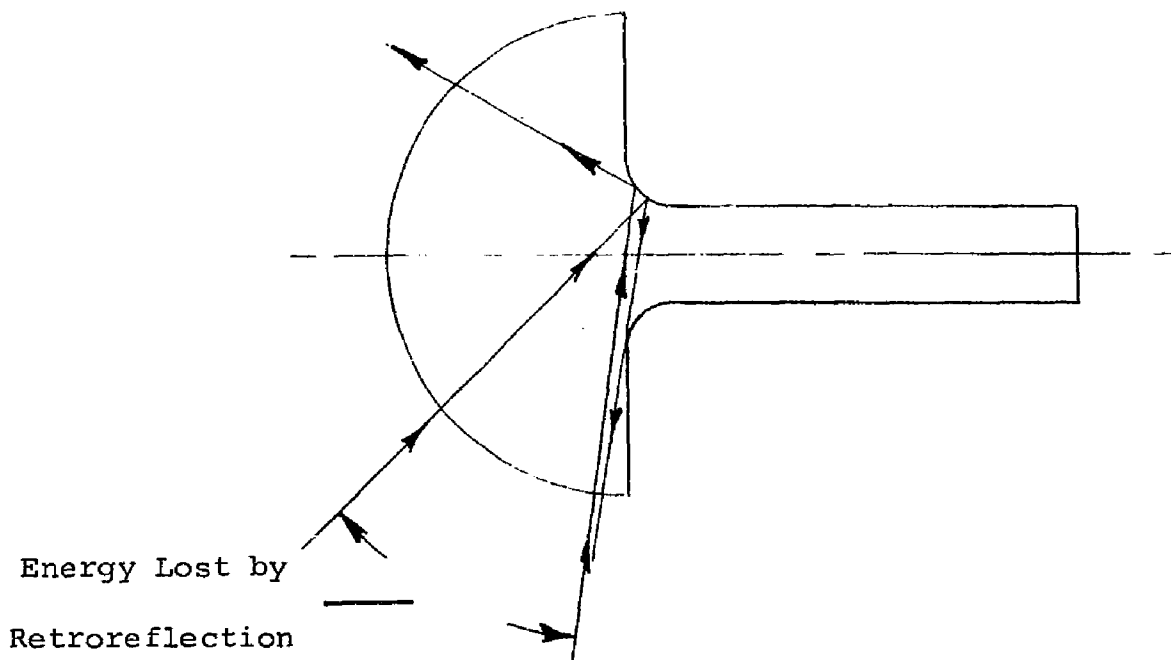


Figure 4. Sketch Showing Retroreflection of Incident Pump Light

To circumvent these lapping difficulties, an alternate design of the optical pumping configuration was made and is illustrated in Figure 5. In this design only the meniscus aplanatic refractor is employed. The hyperhemispherical aplanat is deleted. The optical work the hyperhemispherical lens accomplished is now accomplished by use of a reflecting cone. The entrance aperture of the cone matches the size of the solar image formed by the combination of the parabolic mirror and the meniscus aplanat. The cone condenser is then tapered down to an exit aperture which obeys the relationship:

$$NA_{\text{incident}} \times D_{\text{entrance aperture}} = (NA_{\text{desired}} = 1.9) \times D_{\text{exit aperture}}.$$

This relationship is effective for the axial bundles. For the field bundles, however, substantial vignetting occurs unless a field lens is incorporated at the entrance aperture of the cone condenser. Such a cone condenser, including field lens, was designed. Design considerations included an optimization between the pump energy aberration loss occurring in a large

ALL DIMENSIONS IN mm

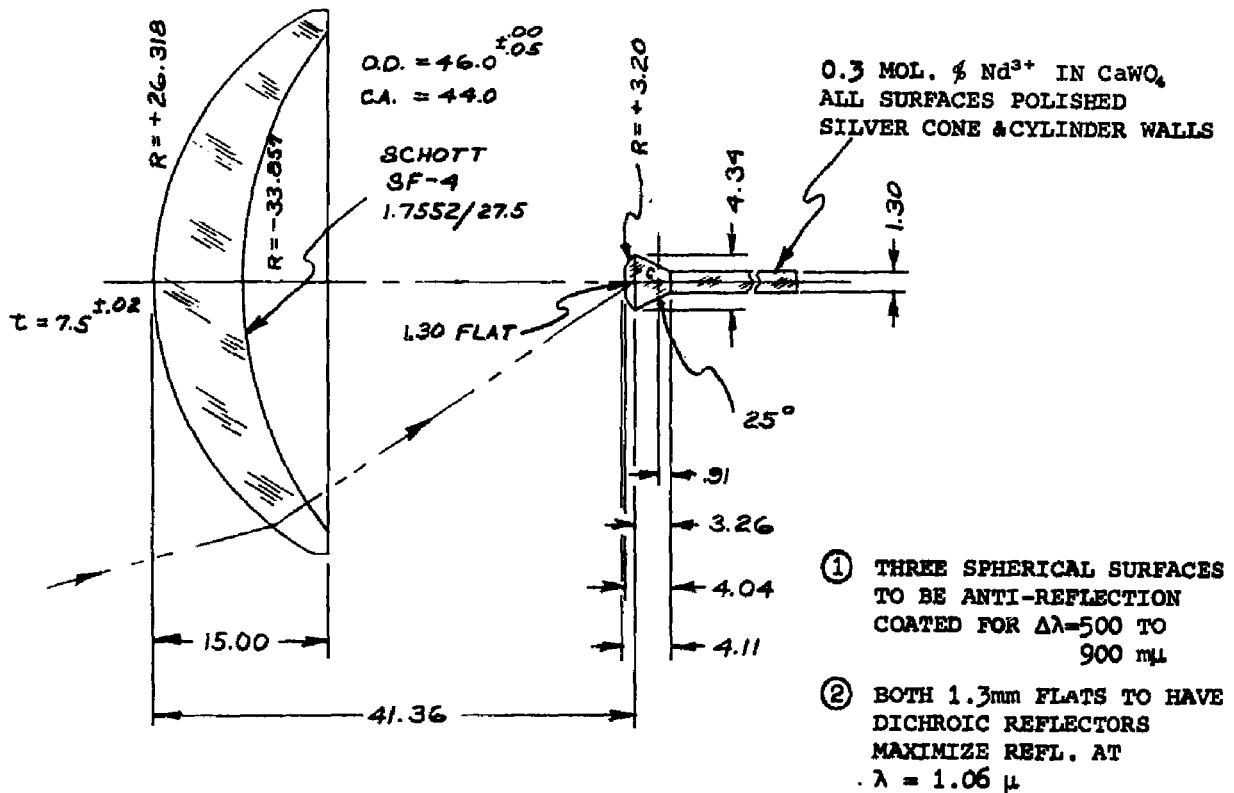


Figure 5. Pump Optics Using Cone Condensor in Place of Hyperhemispherical Aplanat

vertex angle cone condenser and short focal length field lens, and the pump energy lost in a configuration employing a small vertex cone angle and a weak field lens where the path length of the pump energy in the absorbing  $\text{CaWO}_4$  not between the Fabry-Perot mirrors is greater. One can see by inspection that this configuration requires no sharp angle optical lapping. Indeed, a fillet at the intersection of the cylinder and the cone condenser can be employed with negligible pump energy loss. The pump energy vignettted by the front surface Fabry-Perot mirror is approximately the same for the cone condenser configuration as for the hemisphere immersion lens configuration (viz: 7%).

Preliminary calculations have indicated that a substantial portion of the pump energy is absorbed in the highly doped conical element outside of the active region between Fabry-Perot mirrors. This wasted energy is primarily in the yellow region of the spectrum, where the absorption coefficient of a neodymium-doped material is at its maximum; and its magnitude may exceed 30% of the total useful pump energy for a 0.5% doped material. The total pump energy losses in the competing system employing a hyperhemispherical immersion lens are not much smaller, however, because of the Fresnel surface losses at the additional refractor element.

### 2.2.2 Laser Cavity

The diameter of the  $\text{CaWO}_4$  laser cavity has been chosen to be 1.3 mm, a value slightly smaller than the diameter of the sun's image obtained in the laser transmitter system. This image diameter is, of course, determined by the collector mirror diameter and the refractive index of the selected laser material.

$$d_{\text{image}} = \frac{d_{\text{collector}} \times \theta_{\text{sun}}}{2\eta} \approx \frac{600 \text{ mm} \times 0.01}{2 \times 1.92} \approx 1.5 \text{ mm}$$

The length of the laser cavity will be determined by both laser and pumping considerations. That is, it is desirable to make the cavity long (and highly doped) for high utilization of the available pump energy. On the other hand, the increased material, absorption and scattering, losses which result from greater cavity lengths eventually outweigh end mirror losses, and therefore cause an increase in the required level of inversion for laser operation. Cavity length, then, will be chosen separately for each piece of material, based on its doping concentration and measured value of material loss coefficient. It is expected that cavity length for a 0.4% Nd-doped  $\text{CaWO}_4$  of high optical quality will be 1 to 3 cm.

Special processing procedures are necessary to make an optical part of the shape illustrated in Figure 5.

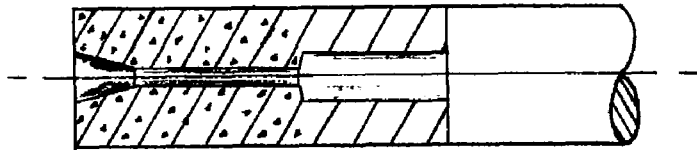


Figure 6. Hollow Milling Tool

The cylindrical-conical piece cannot be produced by conventional methods due to the stresses introduced in the part by generating and polishing operations. Two special techniques for the fabrication of the part have been developed. They are:

- (a) A hollow tool driven by an ultrasonic transducer, used with an abrasive slurry to get cutting action without producing a bending moment.
- (b) A special diamond impregnated hollow milling tool, mounted to be fed axially while the  $\text{CaWO}_4$  rod is rotated at high speed. This method proved to be easier to control than method (a) and had the advantage that the same spindle and alignment "V" block could be used for polishing.

Polishing of the cylindrical and conical surface requires a considerable amount of pressure without introducing a bending moment. This was solved by making a split lap so that pressure could be applied equally on both surfaces as the piece rotated. The mount also provides free rotation about axis "b" and limits the forces introduced by the polishing action to those due to torsion.

These techniques for generating and polishing the laser element in  $\text{CaWO}_4$  were developed using glass as a substitute material. One  $\text{CaWO}_4$  element has been generated successfully from scrap material with the diamond lap technique.

### 2.2.3 Heat Sink and Cooling System

Figure 8 shows the heat sink and heat exchanger system as it has been designed and is being fabricated for the conical shape laser element. In this arrangement, the laser rod is immersed under some pressure in a silver heat sink. The silver sink is surrounded by a finned copper heat exchange chamber, through which is circulated an acetone coolant at  $-100^\circ\text{F}$ . A stainless steel tank containing the acetone and dry ice mixture, and a specially-gasketed pump for circulation of the coolant are mounted externally to the transmitter mount.

Fabrication of the heat sink, and the assembly in it of the laser element introduces a number of problems which require new approaches and techniques for their solutions. For example, the heat sink must be of a highly conductive material, such as silver, in compression at or intimate contact with the laser element surface. This intersurface boundary must be highly reflecting and unbroken, to contain the pump energy within the laser element with minimum loss. Furthermore, immersion of the element within the sink must be accomplished without the introduction of strain and therefore optical distortion in the tungstate element.

The general approach chosen to meet these requirements has involved the design and development of a sintered silver-indium heat sink which is formed around the laser element. The steps in the sintering process are:

- (a) Powdered silver and indium are placed in die cavity, (Figure 9) which contains a steel replica of the  $\text{CaWO}_4$  laser element. Several tons of pressure on the plunger packs the silver mix in a soft cake, B.

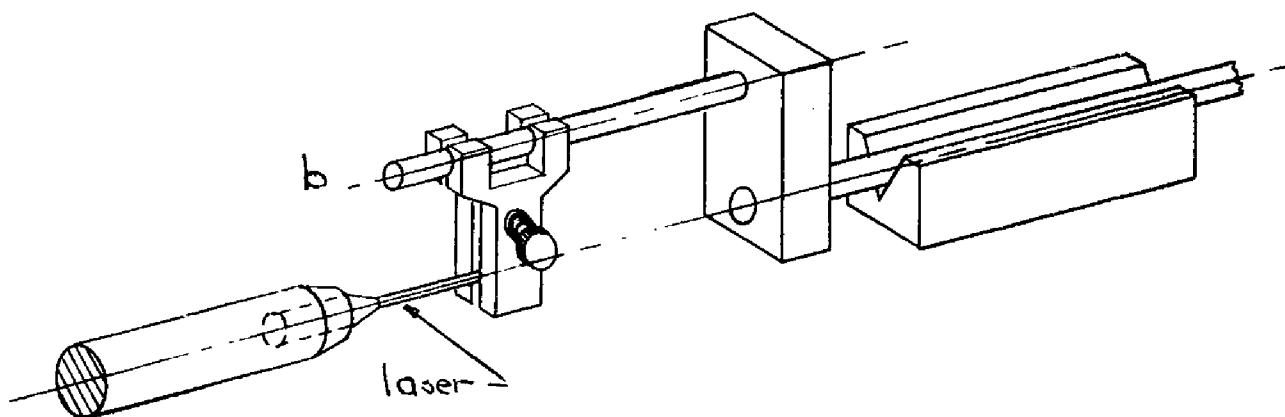


Figure 7. Polishing Lap

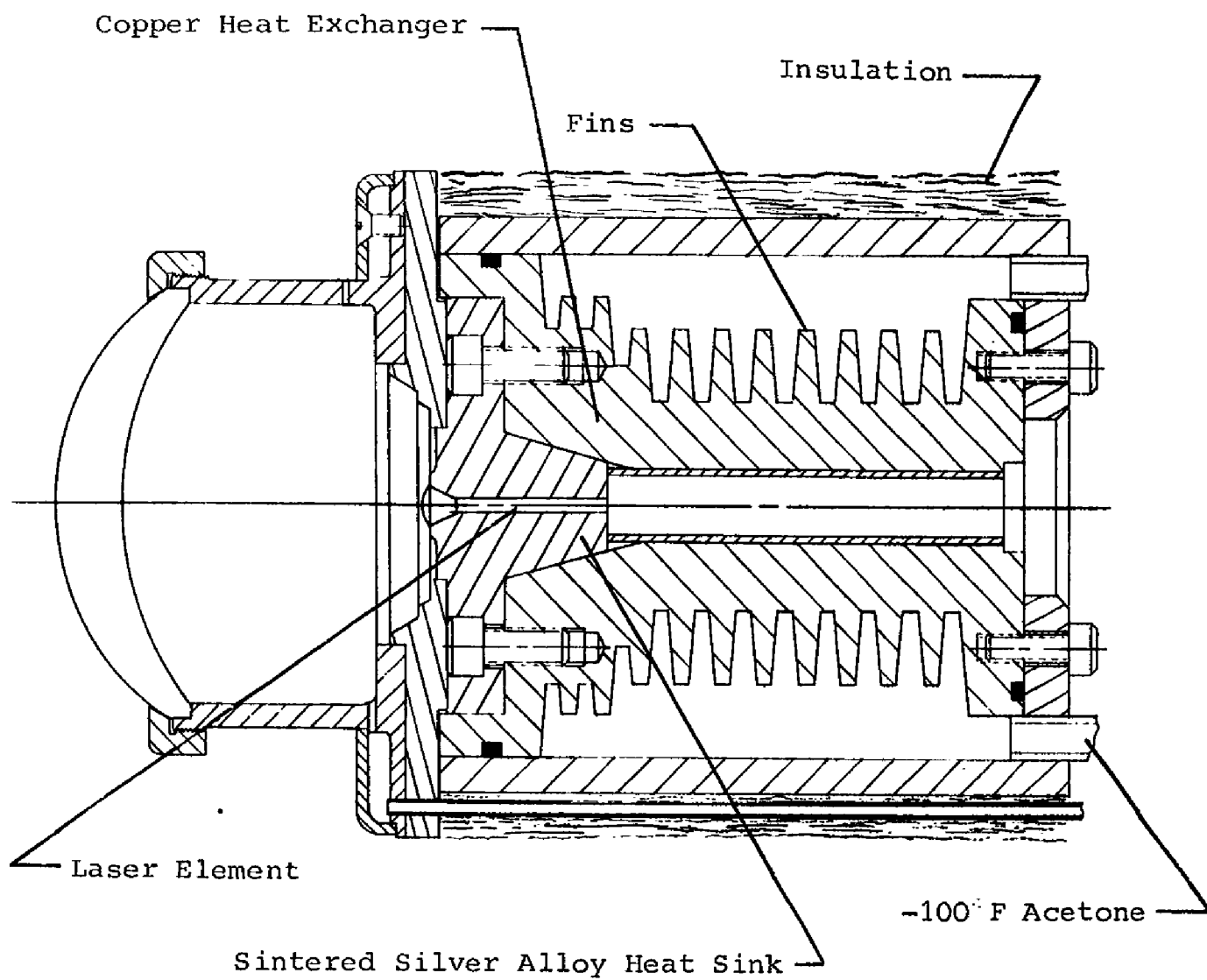


Figure 8. Heat Sink and Heat Exchanger System

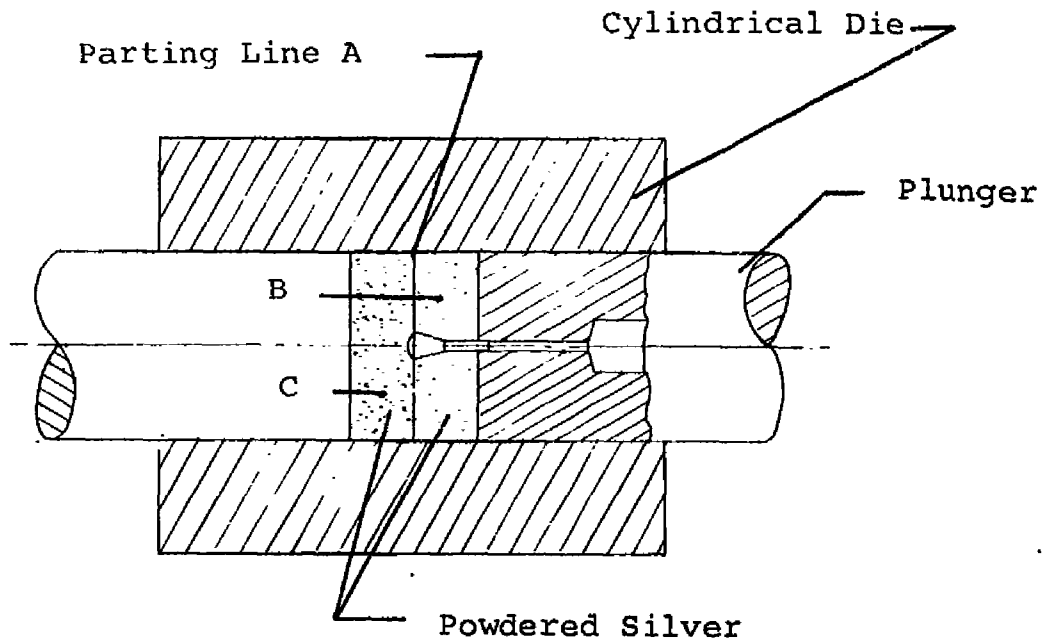


Figure 9. Die Cavity for Forming Sintered Silver Indium Heat Sink

- (b) A parting agent is coated on surface A, silver and indium powder are added and compressed to form cake C.
- (c) The soft silver cakes B and C are removed from the die and the steel replica is replaced by the laser element.
- (d) The elements are then reassembled in the die and bonded under heat and pressure. Sufficient flow is expected under these conditions to minimize the introduction of localized strain in the laser element. Shrinkage of the silver on cooling will introduce compression at the surfaces of the laser element to insure a high thermal conductivity at the boundary interface.



The sintering process described above is being evaluated with glass rods in place of the calcium tungstate element. Although the process shows considerable promise, the technique development will not be considered to be complete until a number of Nd-doped  $\text{CaWO}_4$  lasers have been immersed and evaluated.

In another technique development program, a method has been devised for chemically plating silver over an evaporated silver coating on the laser element, and in this way, building up a thick coating (of about 0.002") with considerable mechanical strength. It is believed that this thick coating is required to survive the sintering operation, while still guaranteeing high reflectivity at the surface interface.

#### 2.2.4 Evaluation of Laser Material

We have been informed by the Solid State Materials Corporation of East Natick, Massachusetts that they have produced samples of 1% Nd-doped  $\text{CaWO}_4$  crystals with thresholds of 2 1/2 to 4 joules electrical input pump energy when placed within a G.E. FT-524 flashtube. A visit was made to this corporation and two samples of 1% Nd-doped  $\text{CaWO}_4$  were borrowed for study. Sample #1, after clearing the end, showed a considerable amount of striation. Sample #2, interestingly enough, is a grown boule of doped material transitioning to an undoped section. This sample showed considerably less striation. Threshold was determined in both samples by side pumping inside an FT-524 flashtube. The better sample had a threshold of approximately 250 joules input, a value considerably above that required for sun power operation. Measurements were taken on the better sample to determine the internal loss coefficient. An active measurement technique was employed as illustrated in the sketch below, (Figure 10). In this technique controlled losses are introduced in the optical path between the removed mirrors by insertion of Fresnel reflectors, and the internal material losses are extrapolated mathematically. The material loss coefficient was measured to be 0.6%/cm, a quite low value.

The supplier, Solid State Materials Corporation, is still attempting to grow a boule of high optical quality and low threshold for our evaluation.

The Linde Corporation is now marketing up to 1% Nd in  $\text{CaWO}_4$  with alledged FT-524 side pumped thresholds ranging from 2 to 10 joules. An order has been placed with them for one 2" x 1/4" rod of 0.3% mol. wt. Nd in  $\text{CaWO}_4$ . Delivery of the Linde rod is expected within the near future. Fabrication will

commence upon receipt to form this boule into the cone condenser immersed cylinder described previously.

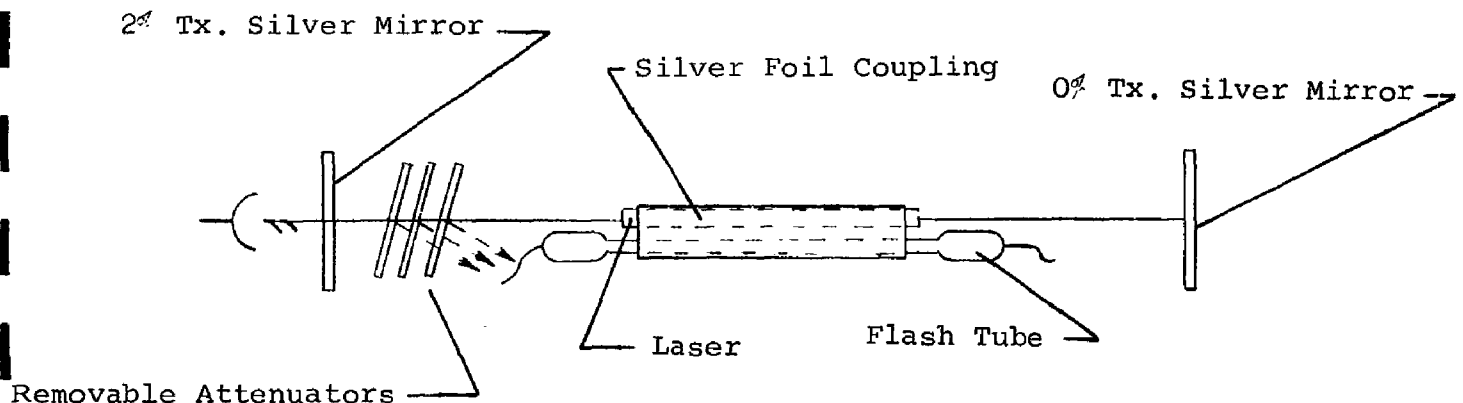


Figure 10. Active Measurement Technique for Determining Internal Loss Coefficients of  $\text{CaWO}_4$  Crystals

#### 2.2.5 Thermal Conductivity Measurements

In order to predict, with some degree of certainty, temperature behavior and heat flow capability for a given heat sink design, some type of measuring apparatus was required which would yield thermal conductivity values for the constituent materials used. A fairly extensive search of the literature was conducted initially and failed to reveal any previous experimental measurement of the thermal conductivity value of  $\text{CaWO}_4$ . Also, as special powdered metal materials would be used in the cooling device, thermal property information could not be appropriately estimated. These materials, used chiefly to aid fabrication procedures, would consist of fine compacted silver or composite material mixtures of indium and silver.

An apparatus was built which would measure the conductivity of specimens to an estimated accuracy of 15%. A somewhat better accuracy might be expected with good conductive

materials and a somewhat higher deviation with poor conductors (crystals, for instance) because of their higher resistance to heat flow and more lossy conditions at the sidewalls. The apparatus was considered adequate, however, for obtaining information needed to perform calculations on the proposed heat sink design.

The apparatus is depicted in Figure 11 and uses a steady-state or constant heat flow method in obtaining thermal conductivity results. The equipment consists, essentially, of two cylindrical copper bars supported in symmetrically opposing fashion on a common longitudinal axis. The heater element is fastened to an end of one of the bars. With the specimen placed at the central gap provided and axial pressure applied, to reduce joint resistance, a continuous heat flow path is established in the bar. Heat is removed at the further end of the opposite bar through a suitable coiled cooling fixture. By mounting on pedestal insulators, the conductors are satisfactorily isolated from the base structure and this serves to minimize heat leakage. When in operation, the test bar between insulator supports is encapsulated within a thick sheath of very low conductivity insulating material to prevent or minimize heat flow.

Temperatures are monitored at six (6) locations along the bar in order to determine the steady-state gradient which occurs under an impressed heat flow. The thermocouples positioned at locations 1, 2, 5 and 6 were cemented into the bar at carefully scaled off distances from the end. Thermocouples 3 and 4 were attached to the edge of thin malleable silver discs which are interposed at the joints between the specimen and copper bar. Two instruments were used to record temperature values: a Leeds and Northrup "Speedomax" strip chart recorder; a Western Electric "Minimite" potentiometer with manual balance.

(a) Experimental Procedure All material specimens, including a copper reference standard were machined to the same dimensional specifications. The apparatus then was calibrated, using the specimen of electrolytic tough pitch copper, the same material used for the conductors bars, and one whose thermal conductivity value is known. With the device assembled, a controlled heat flow was impressed and temperature readings monitored on the strip recorder. After steady state conditions were reached, the pickup was transferred and final temperature measurements were made on the more accurate "Minimite" instrument.

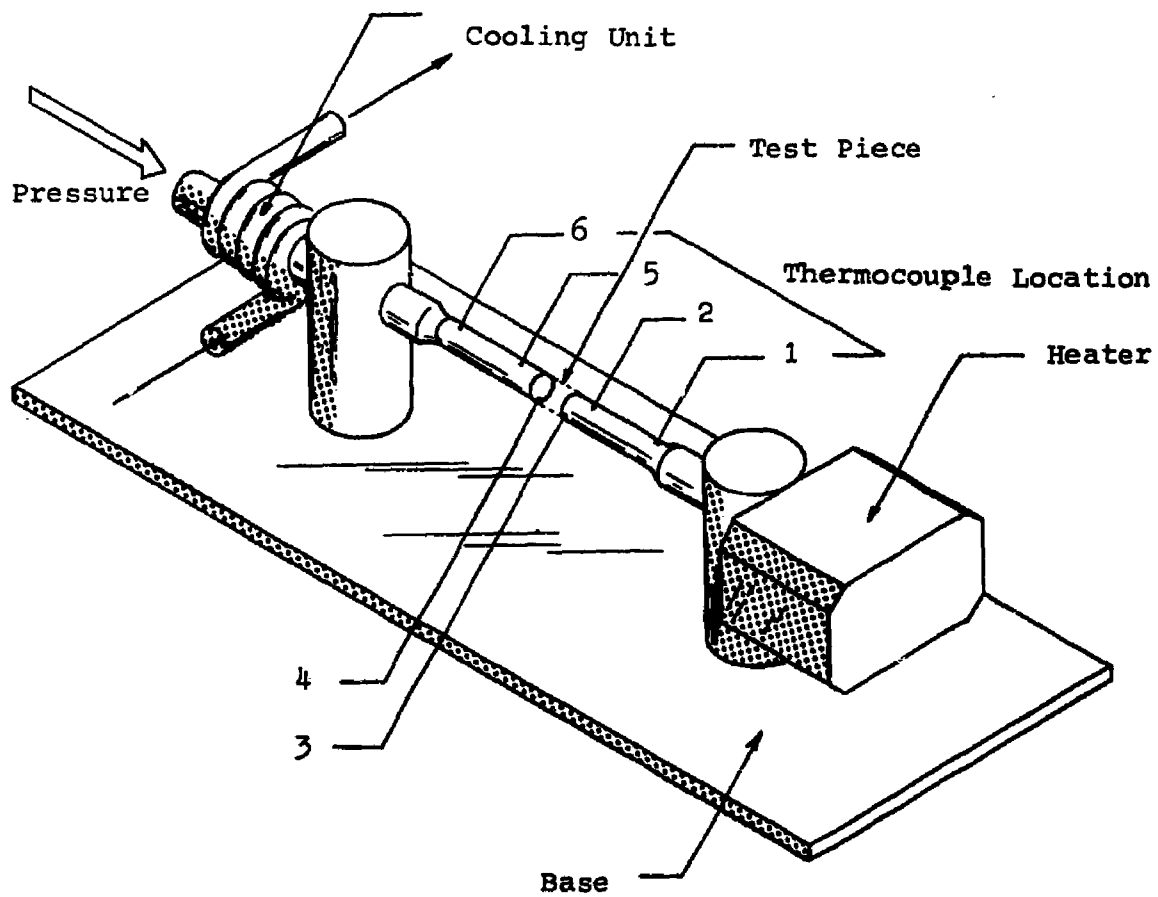


Figure 11. Thermal Conductivity Measurement Apparatus

The axial heat flow between stations 1 and 2 and stations 5 and 6 is given by:

$$Q_{12} = KA \frac{T_2 - T_1}{x_2 - x_1}$$

$$Q_{56} = KA \frac{T_6 - T_5}{x_6 - x_5}$$

The discrepancy between values for  $Q_{12}$  and  $Q_{56}$  is indicative of the radial loss inherent in the system and the arithmetic average gives the axial heat flow through the specimen.

Thus

$$\frac{Q_{12} + Q_{56}}{2} = Q_{34}$$

Temperature drop indicated by the difference,  $T_4 - T_3$ , between the disc thermocouple positions, consists of a cumulative potential drop due to joint resistances at the end surfaces and a specific drop through the specimen itself. We may define, therefore,  $T_4 - T_3$  as a summation  $\Delta T_a + \Delta T_b$  where  $\Delta T_a$  applies to the joint temperature drop alone and  $\Delta T_b$  to the drop in the specimen proper. Since heat flow is essentially constant, we may write:

$$Q_{34} = CA_j \Delta T_a = K_s A_s \frac{\Delta T_b}{x_4 - x_3}$$

Where  $CA_j$  represents a joint factor conductance,  $K_s$  and  $A_s$ , thermal conductivity and cross-sectional area of the specimen, respectively. For a specimen of known conductivity, then, all factors of the equation are determinable for solving for  $\Delta T_b$ .

$$\Delta T_b = \frac{Q_{34} (x_4 - x_3)}{K_s A_s}$$

from which

$$\Delta T_a = \Delta T_{34} - \Delta T_b$$

and the joint factor value becomes

$$CA_j = \frac{Q_{34}}{\Delta T_a}$$

In short, the above procedure utilizes a material of known conductivity to arrive at a joint factor for the system. And it can be assumed this coefficient would remain constant for various materials under study if joint pressure and geometry is reproduced at each experiment. For any complete set of steady-state temperature measurements, then, on a given material, the above system of equations may in turn be evaluated to yield the conductivity value,  $K_s$ . An advantage, obviously, to this technique is that drilling holes and inserting thermocouple probes into the specimen is not required, and interchangeability of materials is readily accomplished.

The value of thermal conductivity of  $\text{CaWO}_4$  as derived by this method was .027 Cal/cm sec $^\circ$ C. which reflects, of course, the radiative component of conduction as well. Mean temperature of the specimen was 300 $^\circ$ F. Results for the compacted silver powder with varying concentrations of indium appeared to be progressively lower when the indium concentration was increased. Also, thermal conductivity depression from pure cast silver seemed significant. This is illustrated in Figure 12 where the data points of the curve were found somewhat scattered. The reason may be attributed to inhomogeneity in the specimen caused by a slight agglomeration of the indium.

#### 2.2.6 Calculation of Temperature Gradients

A calculation of the temperature gradients in a  $\text{CaWO}_4$  system of the hyperhemispherical immersion element type has been performed, and is described in the following section.

As a first step, the irradiance at the laser cavity due to sun pumping has been computed. It is given by the following expression:

$$H = WT (n \sin \theta)^2$$

where

$$H = \text{irradiance, w/cm}^2$$

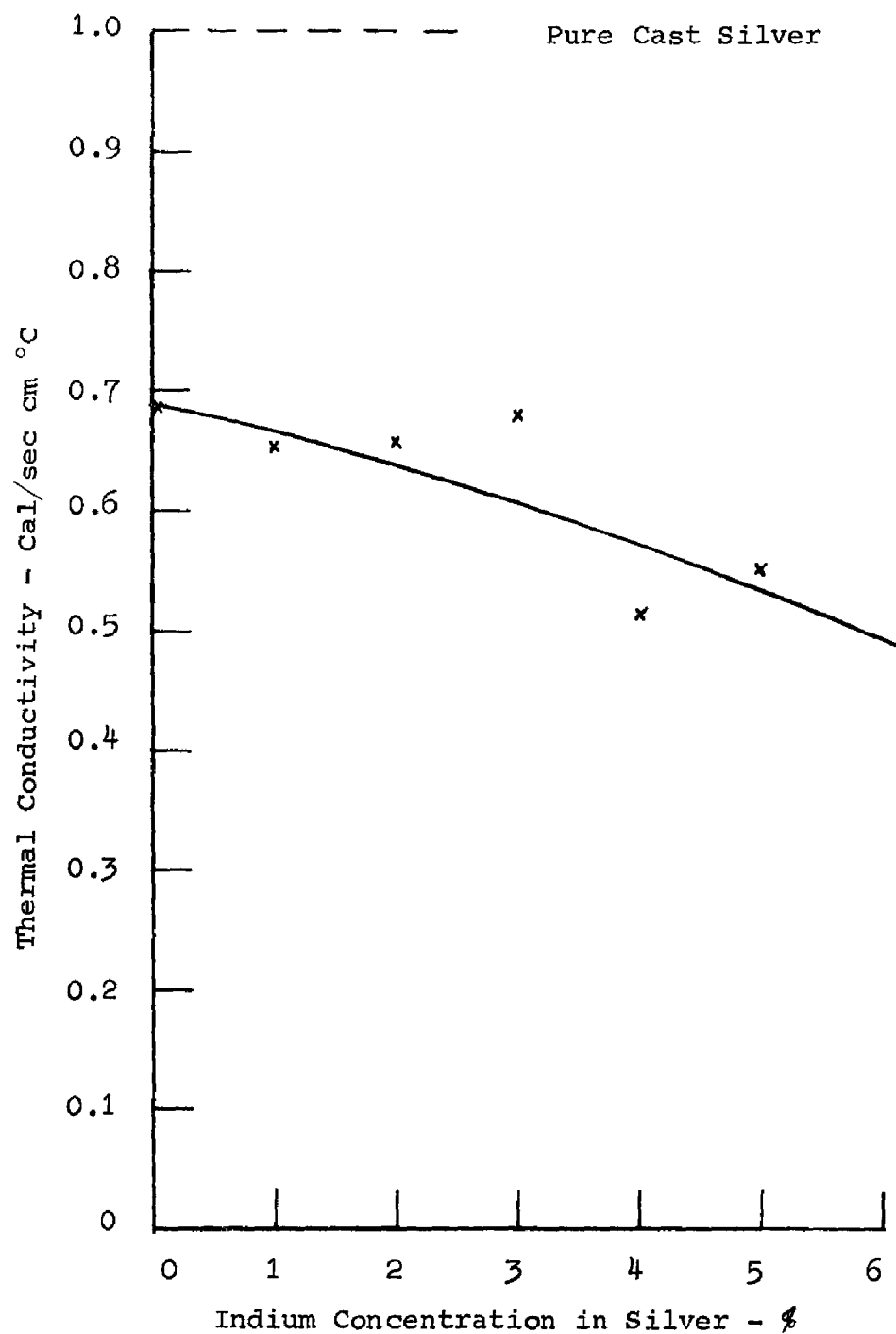


Figure 12. Thermal Conductivity Depression from Pure Cast Silver

$W$  = radiant emittance,  $w/cm^2$

$T$  = transmission of optics

$n$  = immersion index of refraction

$\theta$  = half angle of irradiation.

The transmittance or reflectance of the various optical elements has been taken as

Primary - 0.90

Secondary - 0.94 in  $\Delta\lambda = 500-900 \text{ m}\mu$

- 0.075 elsewhere

First aplanat - 0.96

Second aplanat - 0.93

Immersion Hyper. - 0.93 (assumed undoped)

- .'.  $T = 0.70$

and

$W = 7 \times 10^3 \text{ w/cm}^2$

$W_\lambda = 3.12 \times 10^3 \text{ w/cm}^2$

$n = 1.85$

After correcting for a secondary mirror vignetting of about 8%, the calculated input to the 1.3 mm diameter laser cavity is approximately 100 watts. Since some of this pump power will be absorbed in a doped immersion element, some will be unabsorbed and therefore reflected from the system, and an additional fraction will eventually be reradiated as spontaneous emission, the estimated heat load in the laser cavity has been taken as 50 watts. It is assumed in the following calculations that this load is uniformly distributed through the cavity material, and is removed through the cylindrical side wall of the cavity.

In order to maintain a desirable temperature distribution about the laser cavity, the heat sink was designed cylindrically to preserve radial symmetry. The temperature gradient produced as a result of heat flow in continuous lasering consists of the



cumulative steady-state temperature drop through the resistances of the system to the lowest thermal potential. Referring to the design shown in Figure 9, principal temperature variation will occur across the laser cavity, surface interface, and silver heat sink which extends outward from the cavity.

At the peripheral boundaries of the silver disc the thermal load is transferred to a cylindrical member whose exterior surface consists of integrally fabricated circumferential fins. The fins serve to increase the surface heat transfer area so that heat flowing down the cylinder can be removed effectively to the coolant media. Liquid acetone at  $-65^{\circ}\text{C}$  will be forced circulated around the fins.

The radial temperature distribution in the laser cavity has been calculated by the following formulation:

$$T(r) = T(a) + \frac{\dot{q}}{4K} (a^2 - r^2)$$

Where  $T(a)$  is surface temperature;  $\dot{q}$ , heat generation per unit volume; and  $a$ , outside radius. The value of  $k$ , thermal conductivity, near room temperature, was taken at .04 watts/ $\text{cm}^{\circ}\text{C}$  - a value recently reported for  $\text{CaWO}_4$  by M. G. Holland.<sup>1</sup>

Temperature drop caused by a joint resistance at the surface was calculated from the expression

$$Q = C_j A_s \Delta T$$

where  $Q/A_s$  represents the surface heat flux. The value of  $C_j$ , thermal conductance of the joint, was estimated to be .88 watts/ $\text{cm}^2^{\circ}\text{C}$ . This value, it is felt, is conservative and will probably stand corrected as more accurate information can be obtained.

Radial temperature pattern through the silver heat sink was calculated from

$$T(r) = T(j) - \frac{Q \ln \frac{r}{a}}{2\pi k L}$$

where  $T(j)$  is the joint surface temperature;  $Q$ , the thermal load; and  $L$ , the nominal thickness of the heat sink.  $k$ , the thermal conductivity for the silver heat sink material was taken at .65 Cal/sec  $\text{cm}^{\circ}\text{C}$ , a value experimentally measured.

Composite radial temperature distribution theroretically predicted is plotted in Figure 13. Temperature rise is most significant in the crystal element and across its adjoining interface boundary. This, of course, is principally because of the high flux density and low thermal conductivity of the heat flow path in this area. To achieve an appreciable improvement in the thermal properties of calcium tungstate, low temperature (cryogenic) operating levels would be required.

The remainder of the system was designed to accomplish rapid heat transfer with minimum difference in potential.

(a) Axial Flow. The copper core of the device upon which eleven parallel circular fins are formed, serves to carry heat from the end mounted silver sink and dissipate it to the cooling environment. To formulate the heat flow in this region, a heat balance is described on a differential slice along the axial path. Thus:

$$- KA_c \frac{dT}{dx} = \left[ - KA_c \frac{dT}{dx} - KA_c \frac{d^2T}{dx^2} dx \right] + \eta_f h_c P_e dx (T - T_e)$$

where the three quantities in the expression represent, respectively, heat conducted into the element at position  $x$ , heat leaving the element at  $x + dx$ , and heat removed from the surfaces of the fin in traversing the distance,  $dx$ .  $A_c$  is the cross-sectional area of the cylinder;  $h_c$ , the surface heat transfer coefficient;  $T_e$  the environmental or coolant temperature;  $\eta_f$  and  $P_e$  represent the efficiency and effective parimeter, respectively, of the fin system.

For boundary conditions, we take the temperature at the top of the conductor equal to the copper-silver interface temperature,  $T_s$ ; the temperature at the opposite end is considered to approach that of the coolant. Then a solution to the above differential equation becomes

$$\frac{T - T_e}{T_s - T_e} = e^{-\eta_f h_c P_e / KA_c x}$$

and the heat flow at  $x = 0$  yields

$$q = \int_0^\infty \eta_f h_c P_e (T_s - T_e) e^{-\sqrt{\eta_f h_c P_e / KA_c} x} dx = \sqrt{\eta_f h_c P_e KA_c} (T_s - T_e)$$

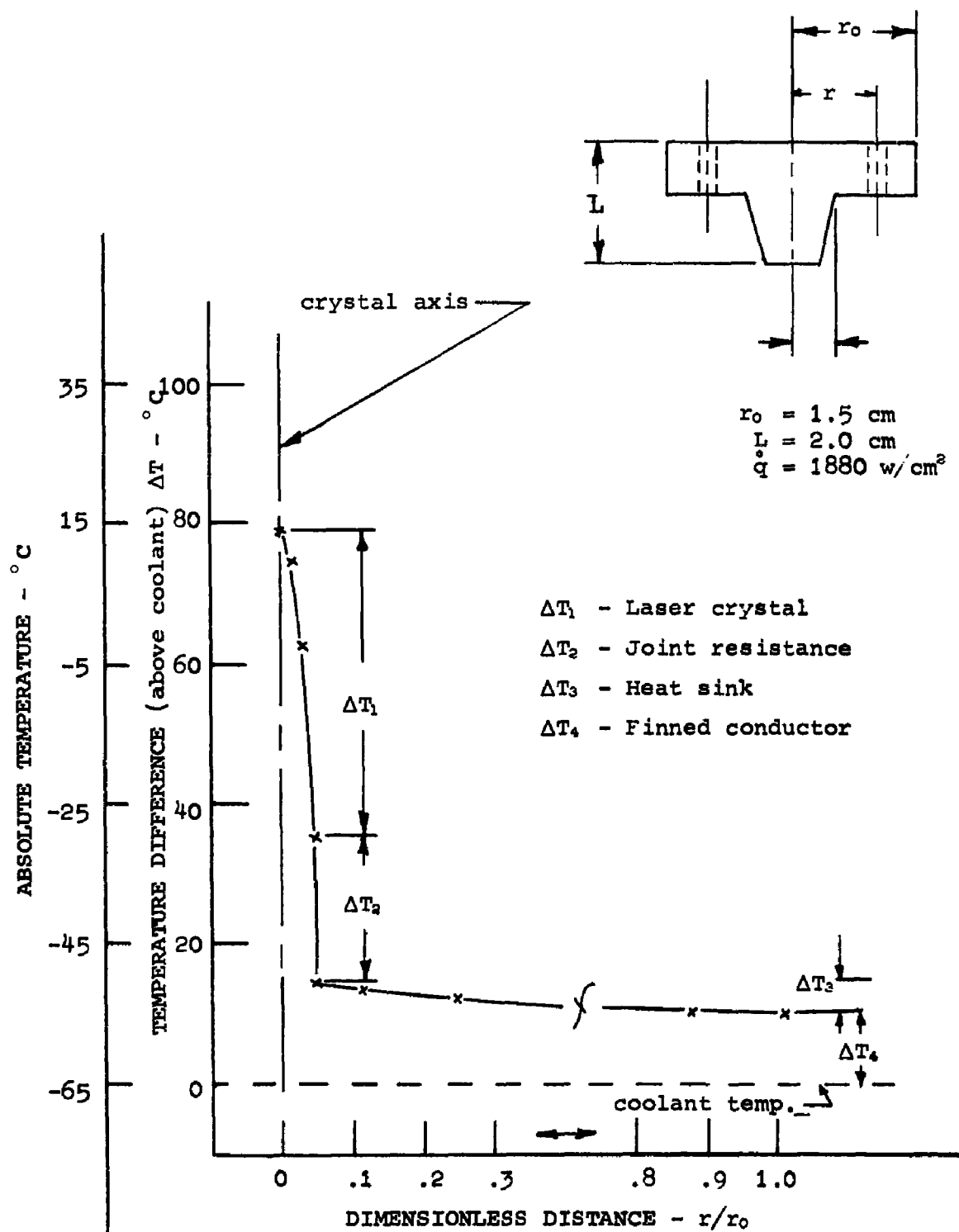


Figure 13. Radial Temperature Distribution

The efficiency of this fin system is determined from the previous work of Gardner<sup>2</sup> and a value is worked out by introducing the design parameters into the prepared curves. This gives an efficiency of 99.4%. The temperature difference,  $T_s - T_e$ , can be numerically evaluated now by knowing or predicting the convective heat transfer coefficient,  $h_c$ . A nominal design value for  $h_c$  was taken at .085 watts/cm<sup>2</sup> °C and the temperature difference calculated to be 7.53° C.

By a similar method used to estimate temperature drop due to joint resistance at the laser sidewall, the value derived for the silver-copper interface was 2.5° C.

(b) Coolant Flow Considerations. A coolant system to operate with liquid acetone has been devised for handling the heat load from the laser transmitter. From an external heat exchange reservoir, the liquid acetone is pumped to the transmitter coolant passage through small feed lines and is returned again to the reservoir. Temperature control is maintained in the reservoir by direct sublimation of dry ice which absorbs the heat picked up in the system. To handle the total heat load, including thermal leakage of the various parts, it is estimated the consumption of dry ice will run approximately 2 lbs. per hour.

For cooling the laser, a flow capability of the system is required which will provide, in turbulent motion, a minimum coefficient,  $h_c$ , of .085 watts/cm<sup>2</sup> °C at the finned heat transfer surfaces. To correlate the heat transfer parameters, we use an expression given by McAdams,<sup>3</sup> and take into account entrance effects and channel curvature by properly modifying the results.

$$\frac{h_c}{C_p G} = 0.023 \left( \frac{\mu}{D_h G} \right)^{0.2} (P_r)^{-2/3}$$

$C_p$ ,  $\mu$ , and  $P_r$  in the above are property values of specific heat, viscosity, and Prandlt Number, respectively, evaluated at the coolant temperature.  $D_h$  is the hydraulic diameter of the flow passage. Since a value for  $h_c$  has been established, the above equation, then, may be solved for mass velocity,  $G$ . This is an important quantity because it yields directly the flow quantity,  $Q$ , necessary to obtain transfer within the laser cooling device.

Thus

$$Q = \frac{GA_c}{P}$$

For our particular system, the flow requirement is approximately 5 GPM, and the flow modulus, as defined by Reynolds Number,

$$\frac{GD_h}{\mu}$$

becomes 12,500.

<sup>1</sup> M.G.Holland, "Thermal Conductivity of Several Optical Maser Materials", Jour. App. Phys., Vol. 33, N.9., Sept. 1962.

<sup>2</sup> K.A.Gardner, "Efficiency of Extended Surfaces", Trans. A.S.M.E., Vol. 67.

<sup>3</sup> W.H.McAdams, "Heat Transmission", McGraw Hill Book Co., New York, N.Y., 1954.

### 3 EXPERIMENTAL Nd-DOPED GLASS LASERS

A significant portion of the contract effort in this present report period has been devoted to a study of the possibilities of neodymium-doped glass as a sun-powered laser material. The following advantages can be cited for Nd-glass:

- 1) operation is at room temperature
- 2) low threshold operation has been obtained (although not equal to the Nd-doped  $\text{CaWO}_4$ )
- 3) glass is easily fabricated into unusual configurations
- 4) the material is readily available.

In another project, operation of a 3 cm long clad Nd-glass fiber laser has been achieved when side pumped with an AG-1 photo flashbulb in a highly reflecting sphere. The color temperature of the flashbulb was determined to be about  $4100^\circ\text{K}$ .

At first thought, one would expect that laser operation of the glass would be straightforward, when pumping from the sun (or sun simulator) of color temperature near  $6000^\circ\text{K}$ . However, a number of other factors must be considered, including fiber length (pumped and unpumped), end mirrors reflectivities, loss coefficient of the laser material, and NA of the pump optics system. The pertinent expression has been developed in Appendix III of Interim Engineering Report #1 as the "figure of merit" equation\*. Two versions of a sun-pumped glass fiber laser are described below.

---

\* 
$$G = \frac{\int F(\nu) T_c(\nu) K(\nu) \phi_1(\nu) d\nu}{V_{\text{act}} \left[ \frac{8\pi\eta^2 \nu^3 \Gamma}{W_c^2 \phi_2} \left( S - \frac{\ln R_1 R_2}{2l_{\text{act}}} \right) \right]}$$

### 3.1 SHORT FIBER LASER

The immersion optics and end-pumping scheme developed for ruby and  $\text{CaWO}_4$  have been modified as illustrated in Figure 14. A hemispherical section has been generated in the back surface of the hyperhemisphere so that the optical system provides an NA of nearly unity. The arc image formed at this position is approximately 6 mm diameter. A hemispherical mirror is positioned as illustrated so that the arc image is reimaged upon itself. Thus, a fiber laser lying in the image plane is illuminated through the  $4\pi$  steradians - a pumping system approximately equivalent to that employed in the flashbulb pumping of the fiber laser.

In evaluating a series of 30 mm long glass clad neodymium fibers, it was found that some were successfully pumped by an AG-1 photo flashbulb while others were not despite the fact that all were cut from the same long fiber. This implies that variation in quality (i.e., stria, bubbles, and inclusions) exist along the length of a drawn fiber. The series of 30 mm fibers were pumped by an E.G. and G. FX-33 flashbulb optically coupled to the fiber by means of a reflecting sphere. Threshold varied by as much as four times among the fibers. It was determined that those fibers having electrical energy input of 2 joules or less could be successfully pumped by an AG-1 flashbulb coupled to the fiber by aluminum foil. A 2 joule threshold 30 mm fiber was cut into 7 mm lengths and the threshold again determined by use of the sphere coupled FX-33. Threshold was found to have increased to 11.8 joules, or a factor of nearly 6 times greater than the same fiber in a 30 mm length. An increase in threshold of 4X would be predicted from the equation which expresses the "general condition for oscillation" (Interim Engineering Report #1).

In the neodymium pumping region, (500 - 900 mμ), the averaged radiant emittance of the carbon arc is at least 3 times that of the AG-1 flashbulb. Thus, for similar pumping systems, a fiber laser having a 6 joule threshold for the FX-33 and coupling sphere could be successfully pumped by the carbon arc. However, since the pumping system employed (Figure 14) had 30% greater reflection and transmission losses than the reflecting sphere, the fiber threshold for FX-33 and associated reflecting sphere would have to be 4.2 joules for laser action to be attained in the carbon arc. Measured threshold of the 7 mm fiber was a factor of 2.8 too high to be successfully lasered by the carbon arc. An experimental attempt to laser the 7 mm fiber was predictably unsuccessful.

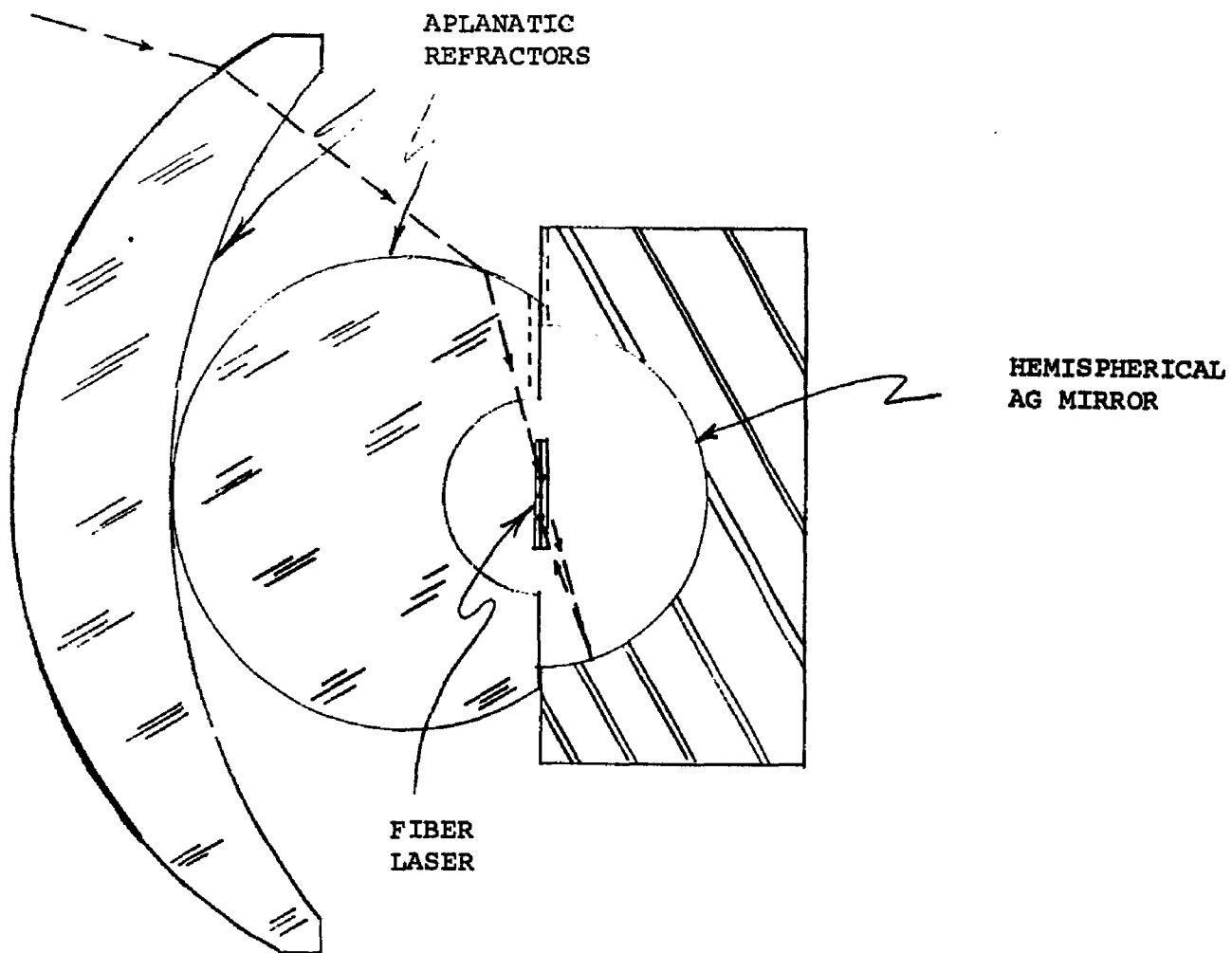


Figure 14. Immersion Optics and End-Pumping Scheme Modified for Nd-doped Fiber Laser



### 3.2 LONG FIBER CONFIGURATION

Again, from the "figure of merit" expression, it can be seen that threshold for a particular material and pumping system can be reduced only by decreasing the end mirror losses, or by increasing the length of laser material which is actively pumped. In the fiber laser experiments described above, the end mirrors were silvered, and mirror loss was estimated to be 3% each. It is possible that a substantial reduction in threshold could be obtained for the short fiber laser, if the ends are coated with low-loss dichroic reflectors. However, in other laser projects at the American Optical Company, dichroics have been very short lived under similar pumping conditions.

A second and perhaps more interesting approach is to devise an optical configuration that will allow the pumping of a longer fiber than that used heretofore. Such a configuration was conceived and is schematically illustrated in Figure 15. The device consists of a hollow glass tube, filled with a liquid of high refractive index, which is transparent to the Nd pump band (500 to 900 mμ). The arc is imaged upon the end of the liquid filled tube. The light is transmitted down the tube without loss by total internal reflection until it hits the silvered end cap on the far end, whereupon it reflects and returns to the entrance pupil and escapes. Nd glass fibers either straight or in bent configuration are immersed within the liquid, as illustrated.

A search for an appropriate liquid promptly yielded  $\text{CCl}_4$  as an excellent candidate.  $\text{CCl}_4$  has a refractive index of 1.46 and is perfectly transparent to the entire Nd pump band. The refractive index of  $\text{CCl}_4$  coupled with that of air yields a NA of entrappment by total internal reflection down the length of the cylinder of 1.0. Thus the fiber can be pumped by a numerical aperture which is nearly equivalent to the  $4\pi$  steradian illumination of the fiber within the reflecting sphere. In the spherical reflector, the NA is unity in one meridian and 1.5 in the other due to the immersion gain of the fiber's glass cladding. This immersion gain is not obtained in the liquid immersed configuration because the liquid index is approximately equal to the index of the cladding glass, thereby removing its optical power. It is possible, of course, to increase the NA of the liquid immersed system to 1.5 in both meridians by silvering the tubing walls, and irradiating the tube end through a high NA immersed optical system. However, multiple reflections of pump energy from the absorbing silvered walls would attenuate the pump energy, so that little, if anything, would be gained over the lower NA total internal reflection scheme.

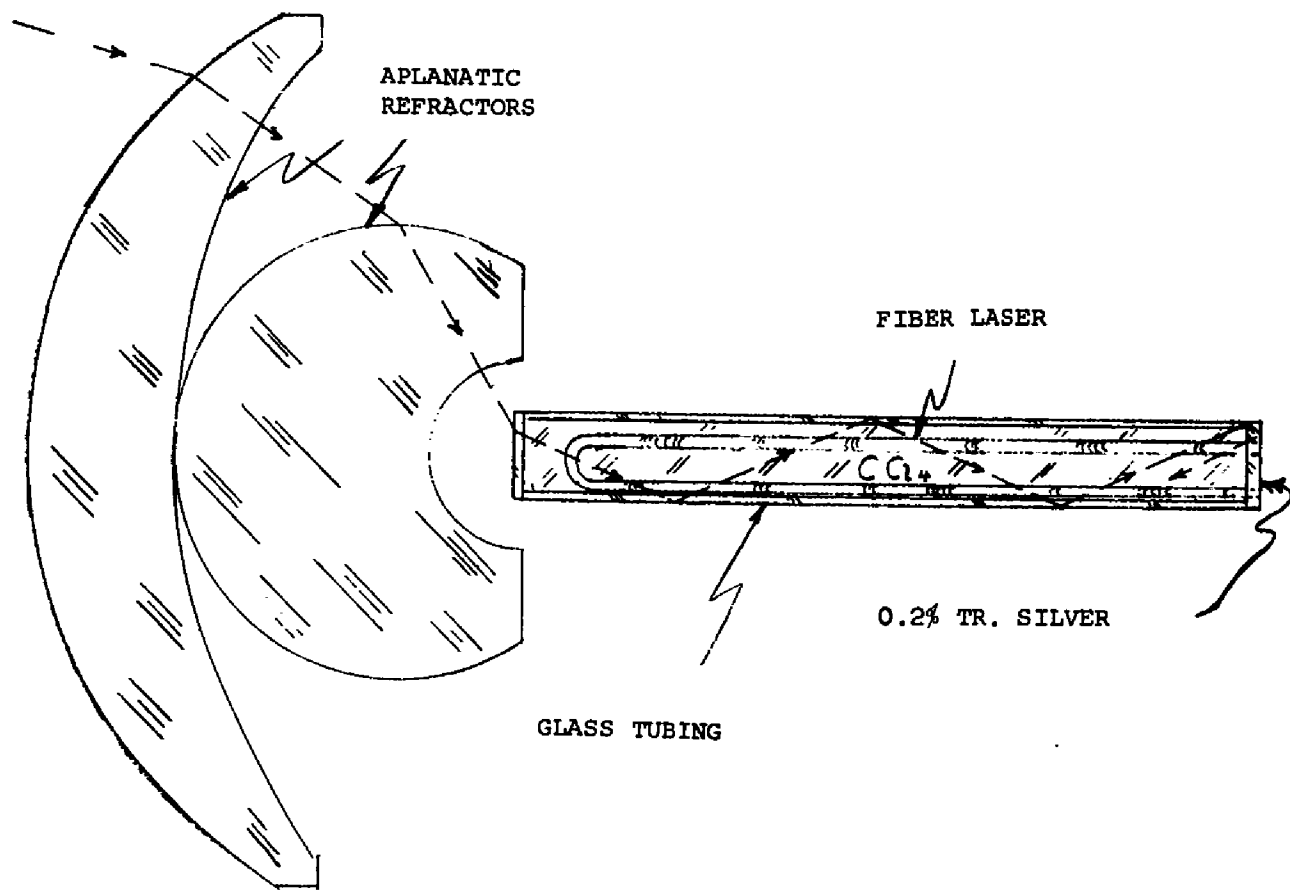


Figure 15. Pump-Optics for Long Fiber

At present, a series of neodymium fibers of 10 to 20 cm in length are being examined for flashtube threshold. Those having the lowest threshold will be selected for carbon arc and solar pumping in the liquid immersion apparatus.